CHEMISTRY OF MATERIALS
Article

Chem. Mater. **2010,** *22,* 1503–1508 1503
DOI:10.1021/cm9027258

Structure and Physical Properties of the Layered Pnictide-Oxides: $(SrF)_2Ti_2Pn_2O$ (Pn = As, Sb) and $(SmO)_2Ti_2Sb_2O$

R. H. Liu, Y. A. Song, Q. J. Li, J. J. Ying, Y. J. Yan, Y. He, and X. H. Chen*

Hefei National Laboratory for Physical Science at Microscale and Department of Physics, University of Science and Technology of China, Hefei, Anhui 230026, People's Republic of China

Received September 2, 2009. Revised Manuscript Received December 13, 2009

The novel family of pnictide-oxides compounds $(SrF)_2Ti_2Pn_2O$ (Pn = As and Sb) and $(SmO)_2Ti_2Sb_2O$ were predicted from the stacking of the well-known fluorite type block $[Sr_2F_2]^{2+}$ or $[Sm_2O_2]^{2+}$ alternating regularly with the anti-CuO_2-type Ti_2O square planar layer and subsequently synthesized. The samples $(SrF)_2Ti_2Pn_2O$ and $(SmO)_2Ti_2Sb_2O$ with an anti-K_2NiF_4 type were characterized by X-ray diffraction, resistivity, susceptibility, Hall coefficient (R_H), thermoelectric power (TEP), and heat capacity. These compounds exhibit an anomalous transition in resistivity and susceptibility at $T_S \sim 380$ K for the As analogue, at $T_S \sim 200$ K for the Sb analogue, and at $T_S \sim 230$ K for $(SmO)_2Ti_2Sb_2O$, respectively, being similar to the anomaly observed in FeAs-based high-T_C parent compounds REFeAsO/AEFeAsF and $AEFe_2As_2$ with a spin density wave (SDW) ordering. A drop in carrier concentration evidenced by a pronounced rise in R_H is observed below T_S for $(SrF)_2Ti_2Sb_2O$. Additionally, TEP changes sign below T_S for $(SrF)_2Ti_2Pn_2O$. Heat capacity demonstrates an anomalous peak at $T_S \sim 198$ K for $(SrF)_2Ti_2Sb_2O$ and $T_S \sim 230$ K for $(SmO)_2Ti_2Sb_2O$, respectively, consistent with that observed in resistivity and susceptibility. Such an anomaly could arise from the SDW/CDW instability or structure distortion. An anomaly associated with the Sm^{3+} ions antiferromagnetic order is observed at 3.2 K in the specific heat for the sample $(SmO)_2Ti_2Sb_2O$.

Introduction

Low-dimensional layered compounds of transition metals have been extensively studied because of their interesting electrical and magnetic properties. The recent discovery of high-T_C in the layered iron-pnictide systems has led to intensively design new layered transition metals pnictide oxides. Actually, a large number of rare-earth or alkaline-earth transition metal oxychalcogenides and oxypnictides have been reported to exhibit layered type intergrowth structures, including the recently discovered FeAs based superconductors. These layered compounds with intergrowth structures can be predicted from the stacking of two-dimensional (2D) secondary building unites (SBUs) of the fluorite type $[Ln_2O_2]$ or $[AE_2F_2]$ (Ln = rare earth elements; AE = alkali earth metal) or one layer of AE^{2+} or double layers of Li^+ or Na^+ alternating regularly with 2D SBUs of the antifluorite $[M_2Q_2]$ (M = D-metal; Q = chalcogenide, pnictide) or the rock-salt $[M_nQ_{n+2}]$ type.[1,2] The numerous variations of elemental combinations in this layered-type intergrowth structure compounds are suitable for their structure−property relationship investigations, such as a structure transition, spin-density-wave (SDW) order, and superconductivity in ZrCuSiAs-type REFeAsO[3−7] or AEFeAsF,[8,9] $ThCr_2Si_2$-type $AEFe_2As_2$,[10−13,15] AFeAs (A = Li, Na),[16] anti-PbO-type FeSe compounds;[17] CDW and superconductivity in Na_xTaS_2[18] and Cu_xTiSe_2.[19,20]

*Corresponding author e-mail: chenxh@ustc.edu.cn.

(1) Kabbour, H.; Janod, E.; Corraze, B.; Danot, M.; Lee, C.; Whangbo, M.-H.; Cario, L. *J. Am. Chem. Soc.* **2008**, *130*, 8261–8270.
(2) Mayer, J. M; Schneemeyer, L. F.; Siegrist, T.; Waszczak, J. V.; Van Dover, R. B. *Angew. Chem., Int. Ed. Engl.* **1992**, *31*, 1645.
(3) Kamihara, Y.; Watanabe, T.; Hirano, M.; Hosono, H. *J. Am. Chem. Soc.* **2008**, *130*, 3296.
(4) Chen, X. H.; Wu, T.; Wu, G.; Liu, R. H.; Chen, H.; Fang, D. F. *Nature* **2008**, *354*, 761–762.
(5) de la Cruz, C.; Huang, Q.; Lynn, J. W.; Li, J.; Ratcliff, W.II; Zarestky, J. L.; Mook, H. A.; Chen, G. F.; Luo, J. L.; Wang, N. L.; Dai, P. *Nature* **2008**, *453*, 899–902.
(6) McGuire, M. A.; Christianson, A. D.; Sefat, A. S.; Sales, B. C.; Lumsden, M. D.; Jin, R. Y.; Payzant, E. A.; Mandrus, D.; Luan, Y. B.; Keppens, V.; et al. *Phys. Rev. B* **2008**, *78*, 094517.
(7) Liu, R. H.; Wu, G.; Wu, T.; Fang, D. F.; Chen, H.; Li, S. Y.; Liu, K.; Xie, Y. L.; Wang, X. F.; Yang, R. L.; He, C.; Feng, D. L.; Chen, X. H. *Phys. Rev. Lett.* **2008**, *101*, 087001.
(8) Matsuishi, S.; Inoue, Y.; Nomura, T.; Yanagi, H.; Hirano, M.; Hosnono, H. *J. Am. Chem. Soc.* **2008**, *130*, 14428.
(9) Wu, G.; Xie, Y. L.; Chen, H.; Zhong, M.; Liu, R. H.; Shi, B. C.; Li, Q. J.; Wang, X. F.; Wu, T.; Yan, Y. J.; Ying, J. J.; Chen, X. H. *J. Phys.: Condens. Matter* **2009**, *21*, 142203.
(10) Rotter, M.; Tegel, M.; Johrendt, D. *Phys. Rev. Lett.* **2008**, *101*, 107006.
(11) Wu, G.; Liu, R. H.; Chen, H.; Yan, Y. J.; Wu, T.; Xie, Y. L.; Ying, J. J.; Wang, X. F.; Fang, D. F.; Chen, X. H. *Europhys. Lett.* **2008**, *74*, 27010.
(12) Sasmal, K.; Lv, B.; Lorenz, B.; Guloy, A.; Chen, F.; Xue, Y.; Chu, C. W. *Phys. Rev. Lett.* **2008**, *101*, 107007.
(13) Wu, G.; Chen, H.; Wu, T.; Xie, Y. L.; Yan, Y. J.; Liu, R. H.; Wang, X. F.; Ying, J. J.; Chen, X. H. *J. Phys.: Condens. Matter* **2008**, *20*, 422201.
(14) Jeevan, H. S.; Hossain, Z.; Kasinathan, D.; Rosner, H.; Geibel, C.; Gegenwart, P. *Phys. Rev. B* **2008**, *78*, 092406.
(15) Chen, H.; Ren, Y.; Qiu, Y.; Bao, W.; Liu, R. H.; Wu, G.; Wu, T.; Xie, Y. L.; Wang, X. F.; Huang, Q.; Chen, X. H. *Europhys. Lett.* **2009**, *85*, 17006.
(16) Chu, C. W; Chen, F; Gooch, M.; Guloy, A. M.; Lorenz, B.; Lv, B.; Sasmal, K.; Tang, Z. J.; Tapp, J. H.; Xue, Y. Y. *Physica C* **2009**, *469*, 326–331.

Published on Web 01/20/2010

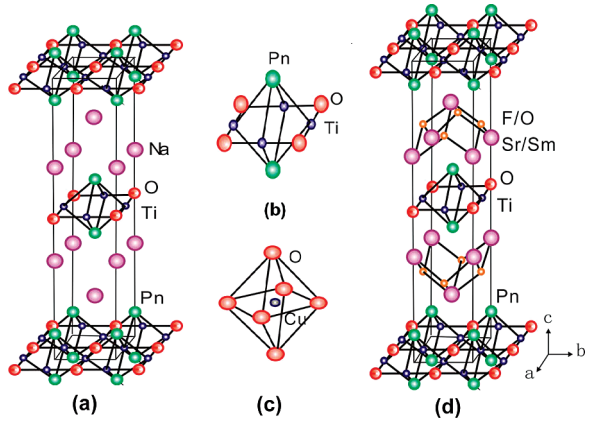

Figure 1. (a) Crystal structure of $Na_2Ti_2Sb_2O$ with the anti-K_2NiF_4 type showing alternation of $[Ti_{4/2}Pn_2O_{4/4}]^{2-}$ layers and double layers of Na^+.[21] (b) The $[Ti_{4/2}Pn_2O_{4/4}]^{2-}$ unit consisting of a Ti−O square plane capped with two Pn^{3-}, and the $Ti_{4/2}O_{4/4}$ square unit is an anticonfiguration to the $CuO_{4/2}$ layer observed in high-T_C cuprates. (c) Structure of the $[CuO_6]$ octahedra unit in high-T_C cuprates $La_{2-x}Ba_xCuO_4$ with the K_2NiF_4 type. (d) Crystal structure of $(SrF)_2Ti_2Pn_2O$ (Pn = As, Sb) and $(SmO)_2Ti_2Sb_2O$ with the anti-K_2NiF_4 type showing an alternation of $[Ti_{4/2}Pn_2O_{4/4}]^{2-}$ layers and the fluorite type $[Sr_2F_2]^{2+}/[Sm_2O_2]^{2+}$ layers.

$Na_2Ti_2Pn_2O$ has been extensively studied because of its charge-density-wave (CDW)/spin-density-wave (SDW) evidenced by the anomalous transition in susceptibility and resistivity.[21,23−27] These behaviors are very similar to that observed in high-T_C iron based oxypnictide parent compounds, such as LnOFeAs (1111) and $AEFe_2As_2$ (122).[13] Powder neutron diffraction showed a tetragonal to orthorhombic structure transition and SDW order in LnOFeAs (1111) and $AEFe_2As_2$ (122), being responsible for the anomaly observed in susceptibility and resistivity.[22] $Na_2Ti_2Pn_2O$ (Figure1a) is an anti-K_2NiF_4 type and crystallizes in *I*4/*mmm* symmetry and edge-shared $[Ti_{4/2}Pn_2O_{4/4}]_n^{2n-}$ layers interspersed by double layers of Na^+. In the $[Ti_{4/2}Pn_2O_{4/4}]^{2-}$ unit (Figure 1b), Ti^{3+} is located between two O^{2-} forming a square planar layer-$Ti_{4/2}O$, and two Pn^{3-} are located above and below the center of the $Ti_{4/2}O_{4/4}$ square unit, which is an anticonfiguration to the $CuO_{4/2}$ layer (Figure 1c) observed in high-T_C cuprates. In the present work, we used the concept of 2D SBUs to predict a new family of pnictide-oxides, $(SrF)_2Ti_2Pn_2O$ (Pn = As, Sb) and $(SmO)_2Ti_2Sb_2O$, in which the double layers of Na^+ are replaced by a fluorite type $[Sr_2F_2]$ or a $[Sm_2O_2]$ layer (Figure 1d). These compounds are isostructural with the $La_2O_2Fe_2OSe_2$[2]/$A_2F_2Fe_2OQ_2$ (A = Sr, Ba; Q = S, Se)[1]compounds. In addition, we systematically studied susceptibility, Hall coefficient (R_H), heat capacity, and thermoelectric power (TEP). These physical properties accompanied with CDW/SDW instability are very helpful for understanding the new family of pnictide-oxides.

Experimental Details

Polycrystalline samples of $(SrF)_2Ti_2Pn_2O$ (Pn = As, Sb) and $(SmO)_2Ti_2Sb_2O$ were synthesized by a solid state reaction method using SrPn, SrF_2 (3N), Sm_2O_3 (3N), TiO_2 (2N), As powder (6N), and Ti (3N) powder as starting materials. SrPn was presynthesized by heating the mixture of Sr (3N) lumps and As (6N) powder or Sb (4N) powder in evacuated quartz tubes at 600 °C for 10 h and at 750 °C for 20 h, respectively. The raw materials were accurately weighed according to the stoichiometric ratio of $(SrF)_2Ti_2Pn_2O$ (Pn = As, Sb) or $(SmO)_2Ti_2Sb_2O$, then thoroughly grounded, and pressed into pellets. The pellets were wrapped with Ta foil and sealed in evacuated quartz tubes. The sealed tubes were sintered at 1000 °C for 50 h for $(SrF)_2Ti_2Pn_2O$ samples and 1150 °C for 50 h for $(SmO)_2Ti_2Sb_2O$ samples, respectively. The sample preparation process except for annealing was carried out in a glovebox in which a high pure argon atmosphere is filled. The obtained black crystalline powder of $(SrF)_2Ti_2Pn_2O$ (Pn = As, Sb) and $(SmO)_2Ti_2Sb_2O$ are stable in air, in contradiction to $Na_2Ti_2Pn_2O$ (Pn = As and Sb) which decomposes to a dark gray phase in a few seconds when the samples are exposed to air.

Phase identification was carried out by X-ray diffraction with MXPAHF 18 kW rotating target X-ray diffractometer (Japan). Data collection was performed at room temperature over a 2θ range of 5−115° with an acquisition time of 7 h. The cell parameters and the crystal structure were refined using the Rietveld method with the programs GSAS package using Thompson-Cox-Hastings functions with asymmetry corrections as reflection profiles. Susceptibility measurement was performed by a SQUID magnetometer (Quantum Design MPMS-XL7s). Hall coefficient (R_H), heat capacity and thermoelectric power (TEP) were measured by using Quantum Design PPMS under fields up to 14 T.

Results and Discussion

A. Structure Refinement. Figure 2 shows X-ray powder diffraction patterns for the samples $(SrF)_2Ti_2Pn_2O$ (Pn = Sb (up panel) and As (down panel)). A few impurity phases of SrF_2 and $SrTiO_3$ are observed in $(SrF)_2Ti_2Pn_2O$. The data were well fitted by a tetragonal $(SrF)_2Ti_2Pn_2O$ phase with the space group of *I*4/*mmm* and SrF_2 and $SrTiO_3$ impurity phases. Rietveld refinement results (the solid line in figure 2) show the good agreement between the data and the calculated profiles. Lattice parameters for the tetragonal unit cell are determined to be a = 4.1095(1) Å and c = 20.8858(5) Å for $(SrF)_2Ti_2Sb_2O$ and a = 4.04865(5) Å and c = 19.4204(2) Å for the As analogue. The results of the Rietveld refinements are listed in Tables 1 and 2. X-ray powder diffraction patterns

(17) Hsu, F.-C.; Luo, J.-Y.; Yeh, K.-W.; Chen, T.-K.; Huang, T.-W.; Wu, P. M.; Lee, Y.-C.; Huang, Y.-L.; Chu, Y.-Y; Yan, D.-C.; Wu, M.-K. *Proc. Natl. Acad. Sci. U.S.A.* **2008**, *105*, 14262–14264.
(18) Gamble, F. R.; Osiecki, J. H.; Cais, M.; Pisharod, R. *Science* **1971**, *173*, 493.
(19) Morosan, E.; Zandbergen, H. W.; Dennis, B. S.; Bos, J. W. G.; Onose, Y.; Klimczuk, T.; Ramirez, A. P.; Ong, N. P.; Cava, R. J. *Nat. Phys.* **2006**, *2*, 544.
(20) Wu, G.; Yang, H. X.; Zhao, L.; Lou, X. G.; Wu, T.; Wang, G. Y.; Chen, X. H. *Phys. Rev. B* **2007**, *76*, 024513.
(21) Axtell, E. A.III; Ozawa, T.; Kauzlarich, S. M.; Singh, R. R. P. *J. Solid State Chem.* **1997**, *134*, 423–426.
(22) Zhao, J.; Adroja, D. T.; Yao, D.-X.; Bewley, R.; Li, S.; Wang, X. F.; Wu, G.; Chen, X. H.; Hu, J.; Dai, P. *Nat. Phys.* **2009**, *5*, 555–560.
(23) Ozawa, T. C.; Pantoja, R.; Axtell, E. A. III; Kauzlarich, S. M.; Greedan, J. E.; Bieringer, M.; Richardson, J. W., Jr. *J. Solid State Chem.* **2000**, *153*, 275–281.
(24) Ozawa, T. C.; Kauzlarich, S. M.; Bieringer, M.; Greedan, J. E. *Chem. Mater.* **2001**, *13*, 1804–1810.
(25) Ozawa, T. C.; Kauzlarich, S. M. *J. Cryst. Growth* **2004**, *265*, 571–576.
(26) Pickett, W. E. *Phys. Rev. B* **1998**, *58*, 4335.
(27) Liu, R. H.; Tan, D.; Song, Y. A.; Li, Q. J.; Yan, Y. J.; Ying, J. J.; Xie, Y. L.; Wang, X. F.; Che, X. H. *Phys. Rev. B* **2009**, *80*, 144516.

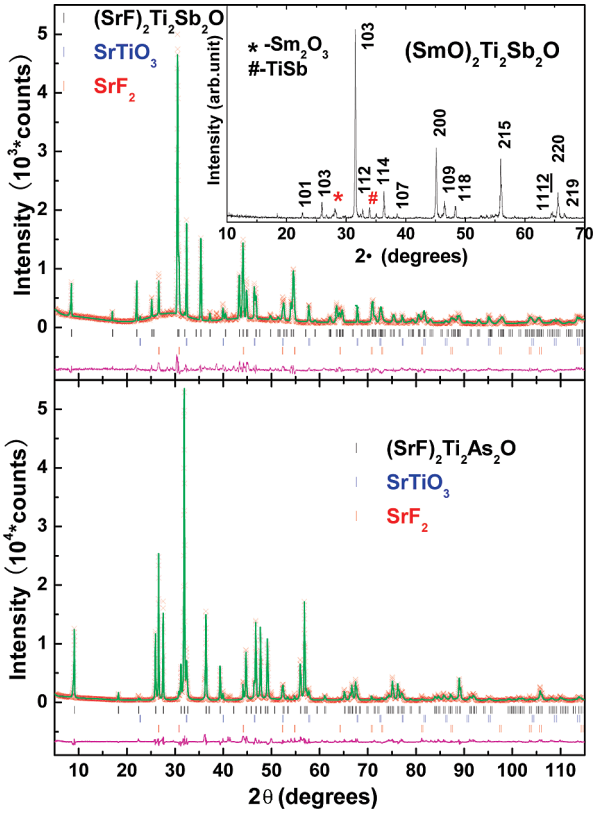

Figure 2. X-ray powder diffraction patterns at room temperature for $(SrF)_2Ti_2Sb_2O$ (top panel) and $(SrF)_2Ti_2As_2O$ (bottom panel). The solid line indicates the intensities calculated using the Rietveld method. The bottom solid curves are the differences between the observed and calculated intensities. The small upper and lower bars indicate the Bragg peak positions of the target compounds and impurity SrF_2 and $SrTiO_3$, respectively. Inset of top panel: X-ray powder diffraction patterns at room temperature for $(SmO)_2Ti_2Sb_2O$.

Table 1. Atomic Coordinates and Equivalent Isotropic Displacement Parameters (U_{iso}) for $(SrF)_2Ti_2Pn_2O$ (Pn = As, Sb)

atom	x	y	z	U_{iso} (Å^2)
		$(SrF)_2Ti_2As_2O$		
Sr	1/2	1/2	0.17767(4)	0.0112(3)
F	1/2	0	1/4	0.0049(2)
Ti	1/2	0	0	0.0006(6)
As	0	0	0.09330(5)	0.0163(4)
O	1/2	1/2	0	0.0328(3)
		$(SrF)_2Ti_2Sb_2O$		
Sr	1/2	1/2	0.18397(9)	0.0210(8)
F	1/2	0	1/4	0.023(4)
Ti	1/2	0	0	0.017(1)
Sb	0	0	0.09673(8)	0.0204(7)
O	1/2	1/2	0	0.0405(7)

at room temperature for a tetragonal $(SmO)_2Ti_2Sb_2O$ phase with the space group of $I4/mmm$ are shown in the inset of Figure 2. Lattice parameters a = 4.032(1) Å and c = 20.153(6) Å for $(SmO)_2Ti_2Sb_2O$ are slightly less than that of $(SrF)_2Ti_2Sb_2O$ because the thickness of the Sm_2O_2 layer is less than that of the Sr_2F_2 layer, similar to that observed in SmOFeAs[7] and SrFFeAs.[8,9]

B. Resistivity and Susceptibility. Figure 3 shows temperature dependence of resistivity for the samples $(SrF)_2Ti_2Pn_2O$ (Pn = As and Sb). The resistivity exhibits a metal-to-insulator transition at about 200 K for $(SrF)_2Ti_2Sb_2O$ and

Table 2. Cell Parameters, Selected Interatomic Distances, Bond Angles and Reliability Factors Obtained Using Rietveld Refinements of $(SrF)_2Ti_2Pn_2O$ (Pn = As, Sb)

	$(SrF)_2Ti_2As_2O$	$(SrF)_2Ti_2Sb_2O$
space group	$I4mmm$	$I4mmm$
a (Å)	4.04865(5)	4.1095(1)
c (Å)	19.4204(2)	20.8858(5)
V (Å^3)	318.33(1)	352.73(2)
Z	2	2
data points	5500	5500
R_{wp} (%)	0.1051	0.0971
R_p (%)	0.0821	0.0741
bond lengths (Å)		
d_{Sr-F}	2.4639(5) × 4	2.4747(11) × 4
d_{Sr-Q}	3.2986(7) × 4	3.4300(14) × 4
d_{Ti-O}	2.02433(3) × 2	2.05480(6) × 2
d_{Ti-Q}	2.7168(7) × 4	2.8816(12) × 4
d_{Ti-Ti}	2.86283(4) × 4	2.90592(8) × 4
bond angles (°)		
Q−Ti−Q	83.66(3) × 2	89.03(5) × 2
	96.34(3) × 2	90.97(5) × 2
O−Ti−O	180 × 1	180 × 1
Q−Ti-O	90 × 8	90 × 8

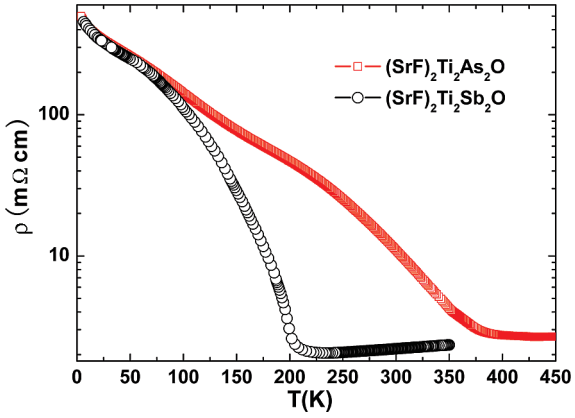

Figure 3. Temperature dependence of resistivity for the samples $(SrF)_2Ti_2Pn_2O$ (Pn = As (square) and Sb (circle)).

at 380 K for $(SrF)_2Ti_2As_2O$, respectively, corresponding to the anomaly in susceptibility. The resistivity increases sharply at a certain temperature, which should be attributed to the opening of a gap.

To study the origin of resistivity anomaly in the samples $(SrF)_2Ti_2Pn_2O$ (Pn = As and Sb), the susceptibility measured under 5T is shown in Figure 4. $(SrF)_2Ti_2Sb_2O$ exhibits a sharp drop in susceptibility around 200 K, and a linear temperature dependent susceptibility from 200 to 300 K and a Curie paramagnetic tail at low temperature. The transition temperature (T_S) is consistent with that observed in resistivity. A similar sharp drop in susceptibility is also observed in As analogues around 380 K, at which the resistivity shows an anomalous transition. The anomaly in susceptibility is similar to that observed in $Na_2Ti_2Sb_2O$ at 115 K and $Na_2Ti_2As_2O$ at 320 K.[21,23−27]

A similar anomalous transition in resistivity and susceptibility can also be found in isostructural $(SmO)_2Ti_2Sb_2O$ as shown in Figure 5. The resistivity exhibits an anomaly at ~230 K for $(SmO)_2Ti_2Sb_2O$, being different from the metal-to-insulator transition at 200 K in $(SrF)_2Ti_2Sb_2O$. The susceptibility shows a slight drop around 230 K as shown in the inset of Figure 5. These behaviors

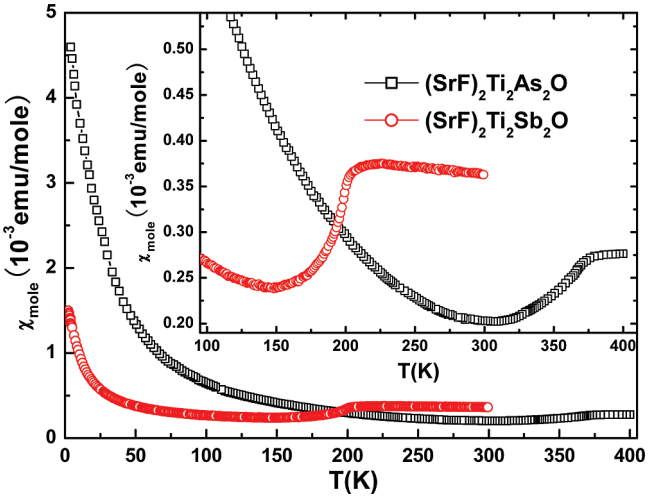

Figure 4. Temperature dependence of susceptibility measured under 5*T* for the samples $(SrF)_2Ti_2Pn_2O$ (Pn = As (square) and Sb (circle)). Inset: the χ vs *T* curve around T_S.

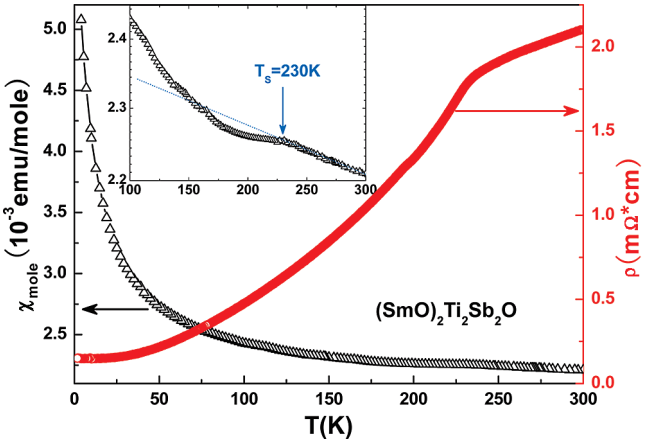

Figure 5. Temperature dependence of resistivity (circle) and susceptibility (up triangle) measured under 5*T* for the samples $(SmO)_2Ti_2Sb_2O$. Inset: the χ vs *T* curve around T_S.

are similar to that observed in $Na_2Ti_2Pn_2O$[27] and quasi-two-dimensional CDW/SDW materials such as high-T_C iron based oxypnictide parent compounds. In FeAs-based parent compounds, these anomalous behaviors observed in resistivity and susceptibility are associated with the structural transition and SDW ordering.[5,6,28,22]

C. Hall Coefficient and Thermoelectric Power. In order to study the type of carriers and the anomalous transition in $(SrF)_2Ti_2Pn_2O$, Hall coefficient (R_H) and thermoelectric power (TEP) are systematically measured. Figures 6 and 7 show the temperature dependence of Hall coefficient (R_H) and thermoelectric power (TEP) for the samples $(SrF)_2Ti_2Pn_2O$ (Pn = Sb and As), respectively. In order to obtain a good and uniform Hall voltage signal, the samples were cut into rectangle shapes with a thickness of 300 μm. The longitudinal and Hall voltages were measured by using the standard dc 6-probe method. The Hall voltage is found to be linear with the magnetic field.

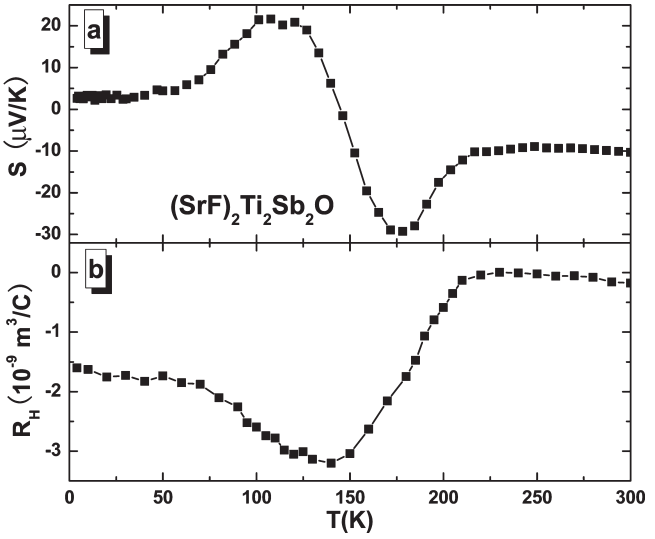

Figure 6. Temperature dependence of thermoelectric power (up panel) and Hall coefficient R_H (down panel) for the samples $(SrF)_2Ti_2Sb_2O$.

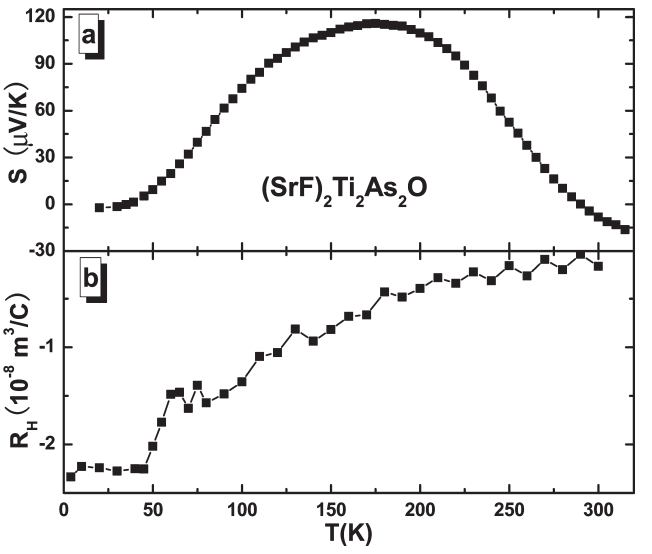

Figure 7. Temperature dependence of thermoelectric power (up panel) and Hall coefficient R_H (down panel) for the samples $(SrF)_2Ti_2As_2O$.

For the sample $(SrF)_2Ti_2Sb_2O$, as shown in Figure 6b, the Hall coefficient is negative and shows a weak temperature dependence above 200 K, indicating that the dominant carrier is electron; and a pronounced rise of the Hall coefficient is observed below T_S. It indicates that the drop in carrier concentration below T_S could arise from the opening of the SDW/CDW gap. It has been revealed that the Hall coefficient is prominently enhanced if strong antiferromagnetic (or SDW) fluctuations exist in heavy-fermion system[29] and iron based oxypnictide parent compounds.[7] Thermoelectric power (TEP) measurements were performed with a Quantum Design PPMS. TEP is negative above 150 K and changes the sign at about 150 K. A minimum around 175 K and a maximum around 110 K are observed. TEP sharply drops around 200 K, coinciding with T_S of the abnormal transition observed in resistivity and the abnormal drop in R_H.

(28) Huang, Q.; Qiu, Y.; Bao, W.; Green, M. A.; Lynn, J. W.; Gasparovic, Y. C.; Wu, T.; Wu, G.; Chen, X. H. *Phys. Rev. Lett.* **2008**, *101*, 257003.

(29) Kontani, H. *Rep. Prog. Phys.* **2008**, *71*, 026501.

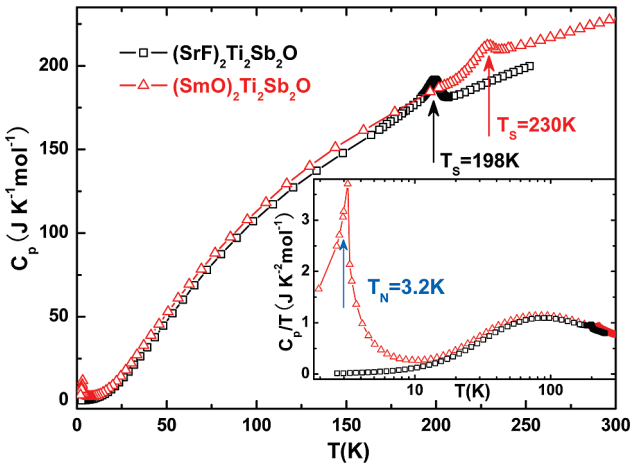

Figure 8. Temperature dependence of specific heat for the sample $(SrF)_2Ti_2Sb_2O$ (square) and $(SmO)_2Ti_2Sb_2O$ (up triangle). For $(SmO)_2Ti_2Sb_2O$ and $(SrF)_2Ti_2Sb_2O$, a clear specific heat jump can be seen at 230 and 200 K, denoted as the CDW/SDW or the structural distortion, respectively. Inset: The sharp peak comes from the antiferromagnetic ordering of Sm^{3+} ions in C_P/T vs ln(T) curve.

Such behavior is quite similar to those of FeAs-based La(1111)[30] and Ba(122)[11−13] systems in which the magnitude of TEP has a visible change at T_{SDW}. It indicates a pronounced change in carrier concentration and multiband behavior. For the As analogue, R_H is negative and monotonously decreases with decreasing temperature. TEP is a small negative at room temperature, and a maximum (115 μV/K) of TEP appears around 175 K. The behavior is similar to that observed in $Na_2Ti_2As_2O$ in which a maximum (70 μV/K) shows up around 125 K.[27]

D. Heat Capacity. In order to study the anomaly observed in susceptibility and resistivity, as FeAs-based oxypnictide with SDW instability[33−35] and CDW/SDW materials,[18−20] the heat capacity was measured by a relaxation-time method with a Quantum Design PPMS. One can clearly see a pronounced anomaly peak of $C_P(T)$ at 198 K for the sample $(SrF)_2Ti_2Sb_2O$ and at 230 K for the sample $(SmO)_2Ti_2Sb_2O$ shown in Figure 8. A clear peak could arise from the typical CDW/SDW instability or a structure distortion. In the low-temperature region the specific heat can be fitted by $C_P = \gamma T + \beta T^3$. The Debye temperature can be estimated from the equation $\beta = (12\pi^4 N k_B)/(5\Theta^3_D)$, where N is the number of atoms per formula unit. From the plot of C_P/T vs T^2 data between 3.1 and 14 K, we can estimate a Sommerfeld coefficient γ = 7.73 mJ K^{-2} mol^{-1}, β = 1.13 mJ K^{-4} mol^{-1}, and Θ_D = 249 K for the sample $(SrF)_2Ti_2Sb_2O$.

(30) Wang, C.; Li, Y. K.; Zhu, Z. W.; Jiang, S.; Lin, X.; Luo, Y. K.; Chi, S.; Li, L. J.; Ren, Z.; He, M.; Chen, H.; Wang, Y. T.; Tao, Q.; Cao, G. H.; Xu, Z. A. *Phys. Rev. B* **2009**, *79*, 054521.
(31) Ghamaty, S.; Lee, B. W.; Markert, J. T.; Early, E. A.; Bjornholm, T.; Seaman, C. L.; Maple, M. B. *Phys. C (Amsterdam, Neth.)* **1989**, *160*, 217.
(32) Cho, B. K.; Kim, J. H.; Kim, Y. J.; Beom-hoan, O; Kim, J. S.; Stewart, G. R. *Phys. Rev. B* **2001**, *63*, 214504.
(33) Ding, L.; He, C.; Dong, J. K.; Wu, T.; Liu, R. H.; Chen, X. H.; Li, S. Y. *Phys. Rev. B* **2008**, *77*, 180510(R).
(34) Baker, P. J.; Giblin, S. R.; Pratt, F. L.; Liu, R. H.; Wu, G.; Chen, X. H.; Pitcher, M. J.; Parker, D. R.; Clarke, S. J.; Blundell, S. J. *N. J. Phys.* **2009**, *11*, 025010.
(35) Rotter, M.; Tegel, M.; Johrendt, D.; Schellenberg, I.; Hermes, W.; Pättgen, R. *Phys. Rev. B* **2008**, *78*, 020503(R).

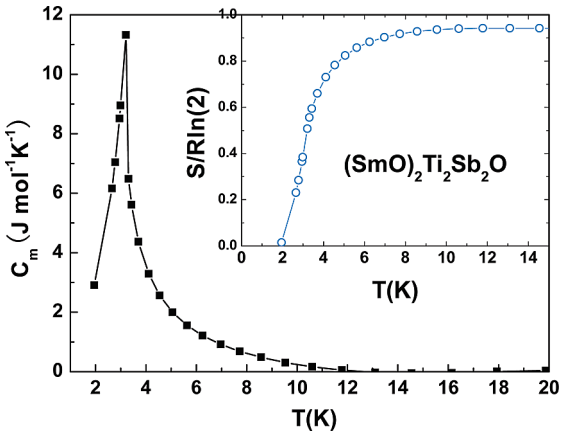

Figure 9. Temperature dependence of magnetic specific heat for the sample $(SmO)_2Ti_2Sb_2O$, $C_m = C - \gamma T - \beta T^3$. Inset: Entropy S_m associated with the ordering of the Sm^{3+} sublattice.

For the sample $(SmO)_2Ti_2Sb_2O$, a pronounced peak at 3.2 K is shown in the inset of Figure 8. In fact, exactly the same specific heat behavior at low temperature has been observed in a tetragonal "T'-phase" structure high-T_C cuprate parent Sm_2CuO_4. Antiferromagnetic ordering of the Sm^{3+} ions in Sm_2CuO_4 at T_N = 5.9 K was proved by the $M(T)$ and $C_P(T)$ measurements.[31] By substituting electron donor element Ce^{4+} for Sm^{3+} ions, the ordering temperature T_N is lowered to 4.7 K in $Sm_{1.85}Ce_{0.15}CuO_4$ with T_C = 16.5 K.[32] Additionally, FeAs-based compound Sm(OF)FeAs[33,34] also shows such similar behavior in specific heat. Since La^{3+} is nonmagnetic, this low temperature peak has not been seen in previous specific heat studies of La(OF)FeAs.[34] Since the same configuration of a Sm_2O_2 layer with the fluorite type in these compounds occurs, the sharp specific heat peak at 3.2 K in $(SmO)_2Ti_2Sb_2O$ manifests the antiferromagnetic ordering of Sm^{3+} ions. Due to the anomalous peak at 3.2 K, it is not easy to extrapolate the electronic coefficient of specific heat γ in the low-temperature limit. The $C(T)$ data between 12 and 24 K can be fitted by the formula $C/T = \gamma + \beta T^2$. It gives the following parameters: γ = 170.15 mJ K^{-2} mol^{-1}, β = 0.72 mJ K^{-4} mol^{-1}, and Θ_D = 289 K for $(SmO)_2Ti_2Sb_2O$. This value of γ is much higher than those obtained in $Na_2Ti_2Sb_2O$ (γ = 12.9 mJ K^{-2} mol^{-1}) and $(SrF)_2Ti_2Sb_2O$ (γ = 7.73 mJ K^{-2} mol^{-1}). Similar values of the γ coefficients (γ = 103.2 mJ K^{-2} mol^{-1}) were reported for $Sm_{1.85}Ce_{0.15}CuO_{4-\sigma}$ with the same building block Sm_2O_2.[32] It is speculated that the effects of magnetic correlation exist well above T_N, thereby it is not easy to make accurate determination of γ.

Figure 9 shows the magnetic specific heat of $(SmO)_2Ti_2Sb_2O$, $C_m = C - \gamma T - \beta T^3$. The magnetic entropy S associated with the antiferromagnetic transition can be evaluated with $S_m = \int C_m/T \, dT$ as shown in the inset of Figure 9. With increasing temperature, the entropy S rapidly increases and saturates to the value of $Rln2$, indicating that the Sm^{3+} ground state in the crystal field is a doublet.

E. Temperature Dependent X-ray Diffraction Patterns. There exists a tetragonal to orthorhombic structure transition corresponding to a SDW order in all FeAs-based high-T_C

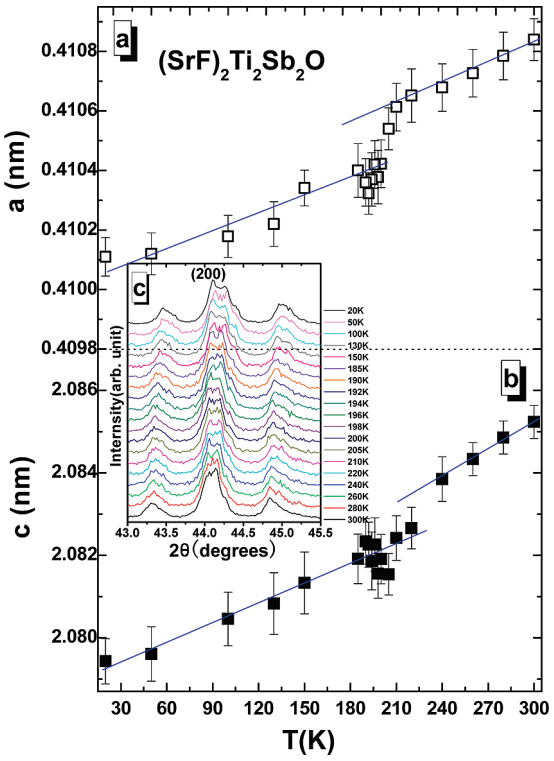

Figure 10. Temperature dependent X-ray diffraction pattern for $(SrF)_2Ti_2Sb_2O$. (a) The lattice parameter *a* as a function of temperature (up panel). (b) The lattice parameter *c* as a function of temperature (down panel). (c) X-ray powder diffraction patterns at near (200) peak at different temperatures.

parent compounds. Furthermore, temperature dependent powder neutron diffraction showed a structural distortion in the $[Ti_2Sb_2O]^{2-}$ layer at SDW/CDW order temperature in $Na_2Ti_2Sb_2O$,[23] being responsible for the anomaly observed in susceptibility, resistivity, and heat capacity. In order to study these anomalous transitions in these compounds, temperature dependent power X-ray diffraction patterns for the sample $(SrF)_2Ti_2Sb_2O$ were measured by MXPAHF 18 kW rotating target X-ray diffractometer. The lattice parameters *a* and *c* as a function of temperature are shown in parts a and b, respectively, of Figure 10. Figure 10a,b indicates a sharp decrease in the lattice parameters *a* and *c* at about 200 K with a slope change, and it suggests a structure distortion at about 200 K, at which the anomalies in resistivity, susceptibility, Hall coefficient, and specific heat are observed. The XRD patterns near (200) peak of $(SrF)_2Ti_2Sb_2O$ at different temperatures were shown in Figure 10c. One could not see that the (200) peak had any splitting below $T_S \sim 200$ K, even at 20 K. The temperature dependent X-ray diffraction data suggest that there is a subtle structural distortion in $(SrF)_2Ti_2Sb_2O$ at $T_S \sim 200$ K. In contrast, all FeAs-based compounds have a distinct structure transition at T_{SDW} or several Kelvins above T_{SDW}. Below T_{SDW}, neutron experiments have confirmed that the Fe^{2+} ions in FeAs layer form the SDW-type antiferromagnetic (AFM) order with direction of magnetic moment along *a*-axis. However, the neutron diffraction and theoretical calculations could not make sure whether there was or not magnetic Ti d^1 ion order in $Na_2Ti_2Pn_2O$. The magnetic moment is expected to be very small, and the structural distortion is subtle in these types of compounds. Even though there are some differences in electronic structure between these compounds and FeAs-based compounds, they both share the common trait of SDW/CDW instability.

Conclusion

In summary, we have synthesized a novel family of compounds, $(SrF)_2Ti_2Pn_2O$ (Pn = As and Sb) and $(SmO)_2Ti_2Sb_2O$, which are isostructural with $A_2F_2Fe_2OQ_2$ (A = Sr, Ba; Q = S, Se) and formed by the stacking of the well-known fluorite type block $[Sr_2F_2]^{2+}/[Sm_2O_2]^{2+}$ layer with an anti-CuO_2-type Ti_2O square planar layer. The samples $(SrF)_2Ti_2Pn_2O$ and $(SmO)_2Ti_2Sb_2O$ with an anti-K_2NiF_4 type were systematically studied by resistivity, susceptibility, Hall coefficient (R_H), thermoelectric power (TEP), and heat capacity. An anomaly in resistivity is observed at $T_S \sim 380$ K for the sample $(SrF)_2Ti_2As_2O$, at $T_S \sim 200$ K for the Sb analogue and at ~230 K for $(SmO)_2Ti_2Sb_2O$, corresponding to the pronounced drop in susceptibility, respectively. These behaviors are quite similar to that observed in $Na_2Ti_2Pn_2O$ (Pn = As and Sb) and FeAs-based parent compounds with SDW instability. Additionally, Hall coefficient R_H and thermoelectric power (TEP) show a pronounced rise at $T_S \sim 200$ K for the sample $(SrF)_2Ti_2Sb_2O$, indicating a drop in carrier concentration at T_S due to the occurrence of possible CDW/SDW. The heat capacity measurement shows a pronounced anomaly peak of $C_p(T)$ at $T_S \sim 198$ K for the sample $(SrF)_2Ti_2Sb_2O$ and at 230 K for the sample $(SmO)_2Ti_2Sb_2O$, corresponding to the typical CDW/SDW instability and a structure distortion. All those results suggest that $(SrF)_2Ti_2Pn_2O$ and $(SmO)_2Ti_2Sb_2O$ are new compounds, being isostructural with $Na_2Ti_2Pn_2O$ with CDW/SDW instability. $(SmO)_2Ti_2Sb_2O$ shows a pronounced peak at 3.2 K in specific heat. As observed in FeAs-based superconducting Sm(OF)FeAs and the electron-doped high-T_C cuprate $Sm_{2-x}Ce_xCuO_{4-\sigma}$, this sharp peak at 3.2 K should be attributed to the Sm^{3+} ions antiferromagnetic order in the $(SmO)_2Ti_2Sb_2O$ system. Temperature dependent X-ray diffraction suggests that $(SrF)_2Ti_2Sb_2O$ has a subtle structural distortion at $T_S \sim 200$ K, corresponding to the CDW/SDW instability. Temperature dependent neutron diffraction experiments are under way to help elucidate the origin of the spin gap behavior and can be used to confirm the existence of the CDW/SDW in these compounds as that of FeAs-based high-T_C parent materials. Additional experiments such as μSR would be the ideal tool to quest for the problem of magnetic ordering in these compounds. Since the SDW/CDW instability is actually believed to be an important prerequisite for superconductivity, our results suggest that $(SrF)_2Ti_2Pn_2O$ and $(SmO)_2Ti_2Sb_2O$ may serve as the parent compounds for novel family of pnictide-oxides superconductors with an anti-K_2NiF_4 structure.

Acknowledgment. This work is supported by the Natural Science Foundation of China and by the Ministry of Science and Technology of China (973 project No:2006CB601001) and by Natural Basic Research Program of China (2006CB922005).